EPiC Series in Engineering
Volume 5, 2023, Pages 61–70
Proceedings of International Symposium on Applied Science 2022

A shear deformable corotational beam element for large displacement analysis of microbeams and microframes

Cong Ich Le[1*], Thanh Tien Pham[2] and Dinh Kien Nguyen[3,4]
[1] Le Quy Don Technical University, 236 Hoang Quoc Viet, Hanoi, Viet Nam
[2] Institute of Applied Mechanics and Informatics, VAST, 291 Dien Bien Phu, Ho Chi Minh city, Viet Nam
[3] Graduate University of Science and Technology, VAST, 18 Hoang Quoc Viet, Hanoi
[4] Institute of Applied Mechanics, VAST, Hanoi
lecongich79@lqdtu.edu.vn

Abstract

The large displacement analysis of microbeams and microframes is presented in this paper via a shear deformable corotational beam element. In order to account for the small size effect, the modified couple stress theory (MCST) is employed in conjunction with Timoshenko beam theory in deriving the internal force vector and tangent stiffness matrix of the beam element. Hierarchical functions are used to interpolate the local displacements and rotation. Newton-Raphson iterative procedure is adopted in combination with the arc-length method to solve the nonlinear equilibrium equation and to trace the equilibrium paths. Various microbeams and microframes are analyzed to show the influence of the size effect on the behavior of the microstructure. The obtained result reveals that the size effect plays an important role on the large deflection response, and the displacements of the structure are overestimated by ignoring the size effect. A parametric study is carried out to highlight the influence of the material length scale parameter on the large displacement behavior of the microbeams and microframes.

1 Introduction

Microbeams and microframes are used in many micro-electromechanical system (MEMS) devices such as capacitive MEMS switches and resonant sensors (Younis, 2011). In MEMS, the microbeams and microframes are often undergone large displacement comparing to their dimensions, and this motivates the geometric nonlinearity analysis of the microstructures. Investigations on buckling and

* Corresponding author

nonlinear behavior of microbeams and microframes have been extensively reported in the last two decades. Contributions that are most relevant to the present work are briefly discussed below.

In order to model the small size effect of microstructures various higher-order continuum theories such as the strain gradient elasticity theory (SGET) (Farokhi, H. and Ghayesh, M. H., 2016), the modified couple stress theory (MCST) (Ghayesh, M. H. and Farokhi, H., 2018) have been developed to accompany a length scale parameter in modeling mechanical behavior of microstructures. Mohammadi and Mahzoon (Mohammadi, H. and Mahzoon, M., 2013) employed both the SGET and MCST to study postbukling of Euler-Bernoulli microbeams under the axial force and temperature rise. Xia et al. (Xia, W., Wang, L. and Yin, L., 2010) developed a new nonlinear beam model for static bending, postbuckling and free vibration analysis of microbeams by introducing a material length scale parameter. The authors showed that the size effect is significant when the ratio of characteristic thickness to the material length scale parameter is approximately equal to one, but is diminishing with the increase of the ratio. Akgoz and Civalek (Akgoz, B. and Civalek, O., 2013) (Akgoz, B. and Civalek, O., 2015) employed the modified strain gradient theory to derive the differential equations for size-dependent buckling analysis of microbeams. The influence of the size effect on the buckling characteristics of the beams was investigated with the aid of the Navier solution technique. The shooting method was employed in conjunction with Newton-Raphson procedure by Wang et al. (Wang, Y.-G., Lin, W.-H. and Liu, N., 2015) in computing nonlinear deflections and post-buckling paths of microscale Euler-Bernoulli beams under the mechanical and thermal loading. Ansari et al. (Ansari, R., Shojaei, M. F., Mohammadi, V., Gholami, R. and Darabi, M. A., 2013), (Ansari, R., Shojaei, M. F. and Gholami, R., 2016) adopted the differential quadrature method and the MCST in their study on nonlinear bending, buckling and vibration of third-order shear deformable functionally graded microbeams. The results of the work reveal that the frequencies buckling loads increase, but the nonlinear-to-linear frequency ratios as well as the deflections decrease by decreasing the thickness-to-material length scale ratio. A total Lagrangian beam element using the fifth-order interpolation was derived by Dadgar-Rad and Beheshti (Dadgar-Rad, F. and Beheshti, A., 2017) for nonlinear bending analysis of microbeams and microframes. The general form of Mindlin's strain gradient theory was adopted by the authors to capture the size effects at micron scales and Newton-Raphson method was adopted to compute the deformation of the mircrobeams and microframes. Attia and Mohamed (Attia, M. A. and Mohamed, S. A. , 2020) investigated the thermal buckling and post-buckling of tapered bidirectional functionally graded microbeams. The governing equations were derived using Reddy beam theory, and then solved by the differential quadrature method in conjunction with the Newton-Raphson method. Numerical investigation perfomed by the authors shows that the material microstructure length scale which modelled via the MCST leads to the higher critical temperatures, but lower deflections.

The von Kármán nonlinear assumption employed in the framework of a fixed coordinate system in the above references enables to model the microstructures with moderate deflections and rotations only. In practice, the microbeams and microframes can undergo large displacements and rotations, and this requires special approach of analysis. The finite element method as a powerful tool in handling nonlinearities is adopted herein to study the size dependent large displacements of planar microbeams and microframes. To this end, a corotational beam element which enables to capture both the small size effect and the large displacements of the microstructure is formulated and used in the study. The element based on Timoshenko beam theory and the MCST is derived by using hierarchical functions to interpolate the displacement field. With the derived element, equilibrium equation in the context of the finite element analysis is derived and solved by the Newton-Raphson based procedure in conjunction with the arc-length method. Numerical investigations are presented to highlight the influence of the size effect on the large displacement behavior of the microbeams and microframes.

2 Timoshenko microbeam model

According to Timoshenko beam theory, axial and transverse displacements, u and w, of a point in a beam element are respectively given by

$$u(x,z)=u_0(x)-z\,\theta(x),\quad w(x,z)=w_0(x) \tag{1}$$

where $u_0(x)$ and $w_0(x)$ are, respectively, the axial and the transverse displacement of a point on the x-axis, and $\theta(x)$ is the cross-sectional rotation.

The shallow arch expression for the axial and shear strains can be adopted for the large displacement analysis as (Crisfield, 1991)

$$\begin{aligned}\varepsilon_{xx}(x,z)&=u_{0,x}(x)+\frac{1}{2}w_{0,x}^2(x)-z\,\theta_{,x}(x)=\varepsilon_0(x)-z\,\theta_{,x}(x),\\ \gamma_{xz}&=u_{,z}+w_{,x}=-\theta+w_{0,x}\end{aligned} \tag{2}$$

with $\varepsilon_0(x)=u_{0,x}(x)+\frac{1}{2}w_{0,x}^2(x)$ is the membrane strain. In Eq. (2) and hereafter, a subscript comma is used to denote the derivative with respect to the followed variable, e.g. $w_{0,x}=\partial w_0/\partial x$.

The constitutive equation based on linearly elastic behavior for the element material is of the following form

$$\begin{Bmatrix}\sigma_{xx}\\ \tau_{xz}\end{Bmatrix}=\begin{bmatrix}E & 0\\ 0 & \psi G\end{bmatrix}\begin{Bmatrix}\varepsilon_{xx}\\ \gamma_{xz}\end{Bmatrix} \tag{3}$$

where σ_{xx} and τ_{xz} are, respectively, the normal and shear stresses, G is the shear modulus and E is the Young's modulus. The shear correction factor ψ in (3) is chosen by 5/6 for the present model.

Since the classical continuum mechanics is not sufficient to predict the size-dependent behavior of micron-scale structures, the MCST proposed by (Yang, F. A. C. M., Chong, A. C. M., Lam, D. C. C. and Tong, P., 2002) is adopted herein to evaluate the strain energy of the microbeam element as

$$U=\frac{1}{2}\int_V(\boldsymbol{\sigma}:\boldsymbol{\varepsilon}+\mathbf{m}:\boldsymbol{\chi})\,\mathrm{d}V \tag{4}$$

where V is the element volume; $\boldsymbol{\sigma}$ and $\boldsymbol{\varepsilon}$ are, respectively, the stress and strain tensors; $\mathbf{m}$ is the deviatoric part of the couple stress tensor and $\boldsymbol{\chi}$ is the symmetric curvature tensor. For the microbeam under consideration, these tensors are given by (Yang, F. A. C. M., Chong, A. C. M., Lam, D. C. C. and Tong, P., 2002)

$$\boldsymbol{\sigma}=\begin{bmatrix}\sigma_x & 0 & \tau_{xz}\\ 0 & 0 & 0\\ \tau_{xz} & 0 & 0\end{bmatrix},\ \boldsymbol{\varepsilon}=\begin{bmatrix}\varepsilon_x & 0 & \gamma_{xz}/2\\ 0 & 0 & 0\\ \gamma_{xz}/2 & 0 & 0\end{bmatrix},\ \boldsymbol{\chi}=\begin{bmatrix}0 & \chi_{xy} & 0\\ \chi_{xy} & 0 & 0\\ 0 & 0 & 0\end{bmatrix},\ \mathbf{m}=2l^2G\boldsymbol{\chi} \tag{5}$$

where

$$\chi_{xy}=-\frac{1}{4}\left(\theta_{,x}+w_{0,xx}\right),\ m_{xy}=2l^2G\chi_{xy} \tag{6}$$

and l is the material length scale parameter; $G=\dfrac{E}{2(1+\upsilon)}$ and υ are shear modulus and Poisson's ratio, respectively. Using Eq. (5), one can rewrite the strain energy for the element in Eq. (4) in the form

$$U=\frac{1}{2}\int_V\left(\sigma_x\varepsilon_x+\tau_{xz}\gamma_{xz}+2m_{xy}\chi_{xy}\right)\mathrm{d}V \tag{7}$$

3 Corotational Timoshenko beam element

3.1 Hierarchical interpolation

The displacements u_0, w_0 of a point on the beam mid-axis and the cross-sectional rotation θ in Timoshenko beam theory are independent, and linear functions can be adopted to interpolate them from their nodal values. The beam element formulated from the linear functions, however suffers from the shear-locking. To avoid the shea-locking problem, the hierarchical functions are employed herein to interpolate the displacement field as (Nguyen, D. K. and Bui, V. T., 2017)

$$u_0 = N_1u_1 + N_2u_2,\ \theta = N_1\theta_1 + N_2\theta_2 + N_3\theta_3,\ w_0 = N_1w_1 + N_2w_2 + N_3w_3 + N_4w_4 \tag{8}$$

where $u_1, u_2, \theta_1, \theta_2, ...w_3, w_4$ are the degrees of freedom and N_1, N_2, N_3 and N_4 are the linear, quadratic, and cubic forms of the hierarchical shape functions with the following forms (Akin, 1994).

$$N_1 = \frac{1}{2}(1-\xi),\ N_2 = \frac{1}{2}(1+\xi),\ N_3 = (1-\xi^2),\ N_4 = \xi(1-\xi^2) \tag{9}$$

With

$$\xi = \frac{2x}{l_e} - 1 \tag{10}$$

being the natural coordinate (with l_e is the initial element length).

A Timoshenko beam element can be formulated from the interpolation (8) and (9). To make the element more efficient, (Tessler, A. and Dong, S. B., 1981) proposed a method by constraining the shear strain to be constant, $\gamma_{xz} = \text{const}$. The method allows to express w_3 and w_4 in term of θ_i (i = 1..3), and the interpolation (8, 9) deduces to the following forms (Nguyen, D. K. and Bui, V. T., 2017)

$$\begin{aligned} u_0 &= \frac{1}{2}(1-\xi)u_1 + \frac{1}{2}(1+\xi)u_2,\ \theta = \frac{1}{2}(1-\xi)\theta_1 + \frac{1}{2}(1+\xi)\theta_2 + (1-\xi^2)\theta_3 \\ w_0 &= \frac{1}{2}(1-\xi)w_1 + \frac{1}{2}(1+\xi)w_2 + \frac{l_e}{8}(1-\xi^2)(\theta_1-\theta_2) + \frac{l_e}{6}\xi(1-\xi^2)\theta_3 \end{aligned} \tag{11}$$

The interpolation (11) is used herein to formulate a size-dependent corotational beam element for large displacement analysis of microbeams and microframes.

3.2 Local and global relationship

A planar 2-node beam element with its kinematics in two coordinate systems, a local (x, z) and a global (X, Z), as depicted in Figure 1 is considered. The element is initially inclined to the X-axis an angle Θ_0. The global system is fixed, while the local one continuously moves and rotates with the element during its deformation. The system (x, z) is chosen such that the origin is at the node 1 and the x-axis directs towards the node 2, so that $u_1 = w_1 = w_2 = 0$. The element vector of local nodal displacements, (**d**), thus contains only four components

$$\mathbf{d} = \{u_2,\ \ \theta_1,\ \ \theta_2,\ \ \theta_3\}^T \tag{12}$$

The global nodal displacements in general are nonzero, and the element vector of global nodal displacements (**D**) has six components as

$$\mathbf{D} = \{U_1,\ \ W_1,\ \ \Theta_1,\ \ \Theta_3,\ \ U_2,\ \ W_2,\ \ \Theta_2\}^T \tag{13}$$

where U_i, W_i, Θ_i (i = 1, 2) are, respectively, the global axial, transverse displacements and rotation at the node i, Θ_3 is a global additional degree of freedom.

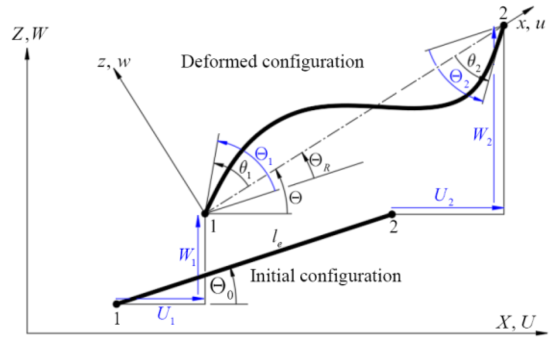

Figure 1: A 2-node corotational beam element and its kinematics

The vectors of nodal internal forces associated with the nodal displacements in Eqs. (12) and (13) are

$$\mathbf{f}_{in} = \{f_u, \quad \mathbf{f}_\theta\}^T, \ \mathbf{F}_{in} = \{\mathbf{F}_U, \quad \mathbf{F}_W, \quad \mathbf{F}_\Theta\}^T \text{ with } f_u = n_2, \ \mathbf{f}_\theta = \{m_1, \quad m_2, \quad m_3\}^T$$
$$\mathbf{F}_U = \{N_1, \quad N_2\}^T, \ \mathbf{F}_W = \{Q_1, \quad Q_2\}^T, \ \mathbf{F}_\Theta = \{M_1, \quad M_2, \quad M_3\}^T \tag{14}$$

where $N_1, N_2, Q_1, Q_2, M_1, M_2, M_3$ are, respectively, the global nodal axial, shear forces and moments at nodes 1 and 2, and similar definition n_2, m_1, m_2, m_3 is applied for the local nodal force and moments.

The following relation between the local displacement and rotations in Eq. (12) with the global ones in Eq. (13) can be obtained from geometric consideration of Figure 1

$$u_2 = l_C - l_e, \ \theta_1 = \Theta_1 - \Theta_R, \ \theta_2 = \Theta_2 - \Theta_R, \ \theta_3 = \Theta_3 - \Theta_R \tag{15}$$

The angle Θ_0, rigid rotation Θ_R, rotation Θ, the initial and current lengths of element l_e, l_C in the above equation are of the following forms (Crisfield, 1991)

$$\Theta_R = \Theta - \Theta_0, \ \tan\Theta_0 = \frac{Z_2 - Z_1}{X_2 - X_1}, \ \tan\Theta = \frac{Z_2 + W_2 - Z_1 - W_1}{X_2 + U_2 - X_1 - U_1}$$
$$l_C = \sqrt{(X_2 + U_2 - X_1 - U_1)^2 + (Z_2 + W_2 - Z_1 - W_1)^2}, \ l_e = \sqrt{(X_2 - X_1)^2 + (Z_2 - Z_1)^2} \tag{16}$$

with (X_1, Z_1) and (X_2, Z_2) are, respectively, the global coordinates of the nodes 1 and 2 of the element in the initial configuration (Crisfield, 1991).

Assuming the strain energy $\mathcal{U}$ of the element has been derived, the global nodal force vector $\mathbf{f}_{\text{in}}$ and the tangent stiffness matrix $\mathbf{k}_{\text{t}}$ for the element can be obtained by successive differentiating $\mathcal{U}$ with respect to the global vector of nodal displacements as

$$\mathbf{F}_{in} = \frac{\partial \mathcal{U}}{\partial \mathbf{D}} = \frac{\partial \mathcal{U}}{\partial \mathbf{d}} \frac{\partial \mathbf{d}}{\partial \mathbf{D}} = \mathbf{T}_1^T \mathbf{f}_{in}, \ \mathbf{K}_t = \frac{\partial^2 \mathcal{U}}{\partial \mathbf{D}^2} = \mathbf{T}_1^T \mathbf{k}_t \mathbf{T}_1 + n_2 \mathbf{T}_2 + (m_1 + m_2 + m_3)\mathbf{T}_3 \tag{17}$$

In the above equations, $\mathbf{f}_{in} = \partial \mathcal{U} / \partial \mathbf{d}$ and $\mathbf{k}_t = \partial^2 \mathcal{U} / \partial \mathbf{d}^2$ are, respectively, the local nodal force vector and tangent stiffness matrix; $\mathbf{T}_1$, $\mathbf{T}_2$ and $\mathbf{T}_3$ are the transformation matrices, which can be computed as

$$\mathbf{T}_1 = \frac{\partial \mathbf{d}}{\partial \mathbf{D}}, \ \mathbf{T}_2 = \frac{\partial^2 u_2}{\partial \mathbf{D}^2}, \ \mathbf{T}_3 = -\frac{\partial^2 \Theta_R}{\partial \mathbf{D}^2}, \tag{18}$$

Eqs. (17) and (18) completely define the element formulation provided that the local nodal force vector and tangent stiffness matrix are known.

3.3 Local formulations

Using the remarked above $u_1 = w_1 = w_2 = 0$ in Eq. (11), one can write

$$u_0 = \frac{1}{2}(1+\xi)u_2 = h_u u_2,\ \theta = \frac{1}{2}(1-\xi)\theta_1 + \frac{1}{2}(1+\xi)\theta_2 + (1-\xi^2)\theta_3 = \mathbf{h}_\theta \boldsymbol{\theta}$$
$$w_0 = \frac{l_e}{8}(1-\xi^2)(\theta_1 - \theta_2) + \frac{l_e}{6}\xi(1-\xi^2)\theta_3 = \mathbf{h}_w \boldsymbol{\theta} \tag{19}$$

where

$$\mathbf{h}_\theta = \left\{\frac{1}{2}(1-\xi),\quad \frac{1}{2}(1+\xi),\quad (1-\xi^2)\right\},\ \mathbf{h}_w = \left\{\frac{l_e}{8}(1-\xi^2),\quad -\frac{l_e}{8}(1-\xi^2),\quad \frac{l_e}{6}\xi(1-\xi^2)\right\}$$
$$\boldsymbol{\theta} = \{\theta_1,\quad \theta_2,\quad \theta_3\}^T \tag{20}$$

Differentiating u_0, θ and w_0 in Eq. (19) with respect to x gives

$$u_{0,x} = b_u u_2,\quad \theta_{,x} = \mathbf{b}_\theta \boldsymbol{\theta},\quad w_{0,x} = \mathbf{b}_w \boldsymbol{\theta},\quad w_{0,xx} = \mathbf{c}_w \boldsymbol{\theta} \tag{21}$$

with

$$b_u = h_{u,x},\ \mathbf{b}_\theta = \mathbf{h}_{\theta,x},\ \mathbf{b}_w = \mathbf{h}_{w,x},\ \mathbf{c}_w = \mathbf{b}_{w,x} \tag{22}$$

The axial strain as given by Eq. (2) and the interpolating functions (19) cannot be used directly to generate a finite element formulation due to the membrane locking effect. In order to avoid this problem, the membrane strain ε_0 in Eq. (2) is replaced by an effective strain defined as (Crisfield, 1991)

$$\varepsilon_{\text{eff}} = \frac{1}{l_e}\int_0^{l_e} \varepsilon_0 \mathrm{d}x = \frac{1}{l_e}\int_0^{l_e}\left(u_{0,x} + \frac{1}{2}w_{0,x}^2\right)\mathrm{d}x \tag{23}$$

Using Eqs. (19) - (22), one can write Eq. (23) in the form

$$\varepsilon_{\text{eff}} = b_u u_2 + \frac{1}{2l_e}\boldsymbol{\theta}^T \int_0^{l_e} \mathbf{b}_w^T \mathbf{b}_w \mathrm{d}x\, \boldsymbol{\theta} = b_u u_2 + \frac{1}{l_e}\boldsymbol{\theta}^T \mathbf{B}_w \boldsymbol{\theta} \tag{24}$$

with

$$\mathbf{B}_w = \frac{1}{2}\int_0^{l_e} \mathbf{b}_w^T \mathbf{b}_w \mathrm{d}x = \begin{bmatrix} l_e/24 & -l_e/24 & 0 \\ -l_e/24 & l_e/24 & 0 \\ 0 & 0 & 2l_e/45 \end{bmatrix} \tag{25}$$

Substituting Eqs. (2), (3), (5), (6) and (19) - (25) into Eq. (7), one gets

$$\begin{aligned} U &= \frac{1}{2}\int_0^{l_e}\Big[EA\left(l_e^{-2}(\boldsymbol{\theta}^T \mathbf{B}_w \boldsymbol{\theta})^2 + 2l_e^{-1}(\boldsymbol{\theta}^T \mathbf{B}_w \boldsymbol{\theta})(b_u u_2) + (b_u u_2)^2\right) + EI\left(\boldsymbol{\theta}^T (\mathbf{b}_\theta^T \mathbf{b}_\theta)\boldsymbol{\theta}\right) \\ &\quad + GA\psi\left(\boldsymbol{\theta}^T (\mathbf{h}_\theta^T \mathbf{h}_\theta)\boldsymbol{\theta} + \boldsymbol{\theta}^T (\mathbf{b}_w^T \mathbf{b}_w)\boldsymbol{\theta} - 2\boldsymbol{\theta}^T (\mathbf{b}_w^T \mathbf{h}_\theta)\boldsymbol{\theta}\right) \\ &\quad + GAl^2\left(0.25\boldsymbol{\theta}^T (\mathbf{b}_\theta^T \mathbf{b}_\theta)\boldsymbol{\theta} + 0.25\boldsymbol{\theta}^T (\mathbf{c}_w^T \mathbf{c}_w)\boldsymbol{\theta} + 0.5\boldsymbol{\theta}^T (\mathbf{b}_\theta^T \mathbf{c}_w)\boldsymbol{\theta}\right)\Big]\mathrm{d}x \\ &= 0.5EA\left(l_e^{-1}(\boldsymbol{\theta}^T \mathbf{B}_w \boldsymbol{\theta})^2 + 2(\boldsymbol{\theta}^T \mathbf{B}_w \boldsymbol{\theta})(b_u u_2) + l_e(b_u u_2)^2\right) + EI\left(\boldsymbol{\theta}^T \mathbf{B}_\theta \boldsymbol{\theta}\right) \\ &\quad + GA\psi\left(\boldsymbol{\theta}^T \mathbf{H}_\theta \boldsymbol{\theta} + \boldsymbol{\theta}^T \mathbf{B}_w \boldsymbol{\theta} - 2\boldsymbol{\theta}^T \mathbf{B}_h \boldsymbol{\theta}\right) + GAl^2\left(0.25\boldsymbol{\theta}^T \mathbf{B}_\theta \boldsymbol{\theta} + 0.25\boldsymbol{\theta}^T \mathbf{C}_w \boldsymbol{\theta} + 0.5\boldsymbol{\theta}^T \mathbf{B}_c \boldsymbol{\theta}\right) \end{aligned} \tag{26}$$

where

$$\mathbf{B}_\theta = \frac{1}{2}\int_0^{l_e} \mathbf{b}_\theta^T \mathbf{b}_\theta \mathrm{d}x = \begin{bmatrix} 1/2l_e & -1/2l_e & 0 \\ -1/2l_e & 1/2l_e & 0 \\ 0 & 0 & 8/3l_e \end{bmatrix},\ \mathbf{H}_\theta = \frac{1}{2}\int_0^{l_e} \mathbf{h}_\theta^T \mathbf{h}_\theta \mathrm{d}x = \begin{bmatrix} l_e/6 & l_e/12 & l_e/6 \\ l_e/12 & l_e/6 & l_e/6 \\ l_e/6 & l_e/6 & 4l_e/15 \end{bmatrix}, \tag{27}$$

$$\mathbf{B}_h = \frac{1}{2}\int_0^{l_e} \mathbf{b}_w^T \mathbf{h}_\theta \mathrm{d}x = \begin{bmatrix} l_e/24 & -l_e/24 & 0 \\ -l_e/24 & l_e/24 & 0 \\ 0 & 0 & 2l_e/45 \end{bmatrix}, \tag{28}$$

$$\mathbf{B}_c = \frac{1}{2}\int_0^{l_e} \mathbf{b}_\theta^T \mathbf{c}_w \mathrm{d}x = \begin{bmatrix} 1/2l_e & -1/2l_e & 0 \\ -1/2l_e & 1/2l_e & 0 \\ 0 & 0 & 8/3l_e \end{bmatrix}, \mathbf{C}_w = \frac{1}{2}\int_0^{l_e} \mathbf{c}_w^T \mathbf{c}_w \mathrm{d}x = \mathbf{B}_c \tag{29}$$

The local internal force vector $\mathbf{f}_{in}$ is obtained by differentiating the strain energy as

$$\begin{aligned} f_u &= \frac{\partial U}{\partial u_2} = AEb_u(u_2 + \boldsymbol{\theta}^T \mathbf{B}_w \boldsymbol{\theta}), \\ \underset{(3\times1)}{\mathbf{f}_\theta} &= \frac{\partial U}{\partial \boldsymbol{\theta}} = AE\left(l_e^{-1} + 2b_u u_2\right)\mathbf{B}_w\boldsymbol{\theta} + 2EI\,\mathbf{B}_\theta\boldsymbol{\theta} + AG\psi\left(2\mathbf{H}_\theta + 2\mathbf{B}_w - 4\mathbf{B}_h\right)\boldsymbol{\theta} \\ &\quad + AGl^2\left(0.5\mathbf{B}_\theta + \mathbf{C}_w + 0.5\mathbf{C}_w\right)\boldsymbol{\theta} \end{aligned} \tag{30}$$

It is convenient to split the local matrix $\mathbf{k}_t$ into sub-matrices as

$$\underset{(3\times3)}{\mathbf{k}_t} = \begin{bmatrix} k_{uu} & \mathbf{k}_{u\theta} \\ \mathbf{k}_{u\theta} & \mathbf{k}_{\theta\theta} \end{bmatrix} \tag{31}$$

The sub-matrices in the above equation have the following form

$$\begin{aligned} k_{uu} &= \frac{\partial f_u}{\partial u_2} = AEb_u,\ \underset{(1\times3)}{\mathbf{k}_{u\theta}} = \frac{\partial f_u}{\partial \boldsymbol{\theta}} = 2AEb_u\boldsymbol{\theta}^T\mathbf{B}_w \\ \underset{(3\times3)}{\mathbf{k}_{\theta\theta}} &= \frac{\partial \mathbf{f}_\theta}{\partial \boldsymbol{\theta}} = AE(l_e^{-1} + 2b_u u_2)\mathbf{B}_w + 2EI\,\mathbf{B}_\theta + AG\psi(2B_w - 4B_h + 2H_\theta) \\ &\quad + AGl^2(\mathbf{B}_c + \mathbf{B}_\theta/2 + \mathbf{C}_w/2) \end{aligned} \tag{32}$$

With the derived local internal force vector $\mathbf{f}_{in}$ and the tangent stiffness matrix $\mathbf{k}_t$, Eqs. (17) and (18) completely define the beam element.

4 Numerical examples

Numerical examples are presented in this section to show the performance of the derived element. For the convenience of discussion, the following dimensionless parameters are introduced

$$U^* = \frac{U}{L},\ W^* = \frac{W}{L},\ \eta = \frac{l^2 GA}{EI},\ P^* = \frac{PL^2}{EI},\ M^* = \frac{ML}{EI} \tag{33}$$

with GA and EI are the shear and bending rigidities, respectively.

4.1 Accuracy and convergence studies

Since the data for large displacements of microbeams and microframes are not available in the literature, the accuracy of the derived formulation is verified herewith by comparing the large displacements of macroframe structure obtained herein by setting $\eta = 0$ with the published data. To this end, Figure 2 and Figure 3 compare the load-displacement curves of a cantilever beam and Lee's frame, respectively. Good agreement between is noted from the figures.

Figure 4 and Figure 5 show convergence of the derived formulation of the derived element in large displacement of the cantilever microbeam and Williams' microtoggle, respectively. The convergence, as seen from the figures, is achieved by using two elements for the cantilever microbeam and only one element per beam for Williams' microtoggle.

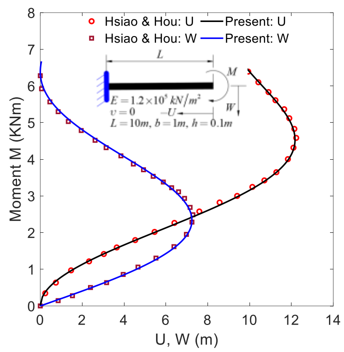

Figure 2: Comparison of tip response of cantilever macrobeam due to a tip moment

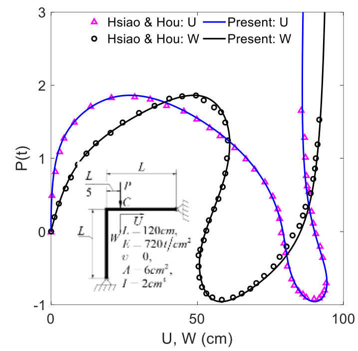

Figure 3: Comparison of load-deflection curves for Lee's macroframe.

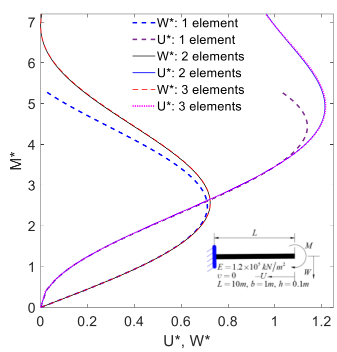

Figure 4: Convergence of the derived formulation in evaluating tip displacements of cantilever microbeam due to a tip moment for $\eta = 0.1$.

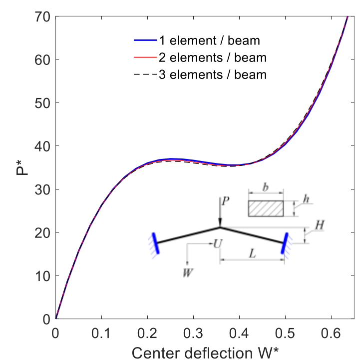

Figure 5: Convergence of the derived formulation in evaluating center deflection of Williams' microtoggle for $\eta = 0.1$.

4.2 Cantilever microbeam with an end moment

A cantilever microbeam under a tip moment M is considered. In Figure 6, the deformed configurations of the microbeam at the value of the length scale and applied moment parameters are depicted for various values of the scale parameter η and loading parameter λ. The microbeam rolls toward a circle when increasing the applied moment. The effect of the material length scale parameter η on the load-displacement curves of the microbeam is shown in Figure 7. As seen from the figure, the parameter η has a significant influence on the large displacements, and the displacements are lower with the presence of the length scale parameter η.

4.3 Lee's microframe

The large displacements of an asymmetric miroframe under a downward P in Figure 3 are investigated herewith. The influence of the size effect and the large displacement behavior of the microframe can be seen from Figure 8, where the load-displacement curves of the microframes are depicted. The limit load of the microframe, as seen from Figure 8 is considerably underestimated by ignoring the size effect of the microframe.

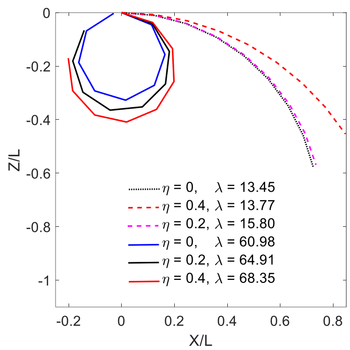

Figure 6: Deformed configurations of cantilever microbeam under tip moment.

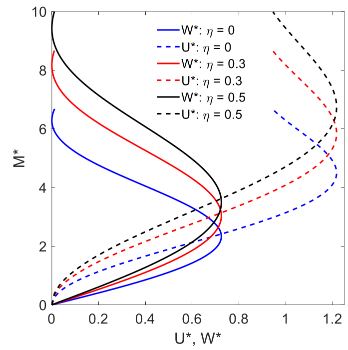

Figure 7: Effect of length scale parameter η on load-displacement curves of cantilever microbeam.

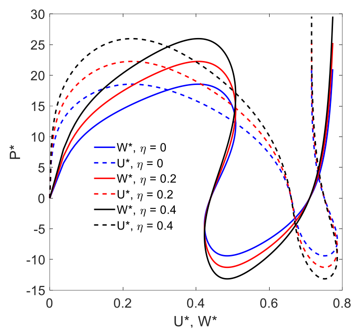

Figure 8: Effect of material length scale parameter η on load-displacement curves of Lee's microframe.

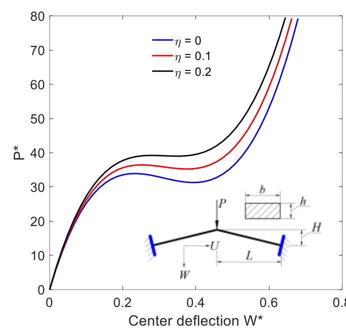

Figure 9: Effect of material length scale parameter η on load-displacement curves of Williams' microtoggle.

4.4 Williams' microtoggle

The Williams' microframe is analyzed by using only two elements per beam with the various values of the material length scale parameter, η = 0, 0.1, 0.2, and the result is shown in Figure 9. As can be observed that the deflection is larger for a smaller value of η. This reveals that the size effect plays an important role in the large displacement behavior of the microstructures, and the displacements are underestimated by ignoring the size effect.

5 Conclusions

A corotational beam element for large displacement analysis of microbeams and microframes was formulated in the basis of Timoshenko beam theory and the MCST. The hierarchical functions were employed in deriving the internal force vector and tangent stiffness matrix of the element. Using the derived element, the equilibrium paths of various microbeams and micro frames have been computed. The obtained results show the derived beam element is accurate and it is capable to model the size effects of the microstructures. The influence of the material length scale parameter on the large displacement behavior of various microbeams and microframes has been examined in detail and highlighted.

References

Akgoz, B. and Civalek, O. (2013). Buckling analysis of functionally graded microbeams based on the strain gradient theory. *Acta Mechanica, 224*(9), 2185–2201.

Akgoz, B. and Civalek, O. (2015). A novel microstructure-dependent shear deformable beam model. *International Journal of Mechanical Sciences, 99*, 10-20.

Akin, J. E. (1994). *Finite elements for analysis and design.* London: Academic Press, Ltd.

Ansari, R., Shojaei, M. F. and Gholami, R. (2016). Size-dependent nonlinear mechanical behavior of third-order shear deformable functionally graded microbeams using the variational differential quadrature method. *Composite Structures, 136*, 669–683.

Ansari, R., Shojaei, M. F., Mohammadi, V., Gholami, R. and Darabi, M. A. (2013). Buckling and postbuckling behavior of functionally graded timoshenko microbeams based on the strain gradient theory. *Journal of Mechanics of Materials and Structures, 7*(10), 931-949.

Attia, M. A. and Mohamed, S. A. . (2020). Nonlinear thermal buckling and postbuckling analysis of bidirectional functionally graded tapered microbeams based on Reddy beam theory. *Engineering with Computers*, 1-30.

Crisfield, M. A. (1991). *Non-linear finite element analysis of solids and structures. Volume 1: Essentials.* New York: Wiley.

Dadgar-Rad, F. and Beheshti, A. (2017). A nonlinear strain gradient finite element for microbeams and microframes. *Acta Mechanica, 228*(5), 1941-1964.

Farokhi, H. and Ghayesh, M. H. (2016). Size-dependent behaviour of electrically actuated microcantilever-based MEMS. *International Journal of Mechanics and Materials in Design, 12*(3), 301-315.

Ghayesh, M. H. and Farokhi, H. (2018). Nonlinear behaviour of electrically actuated microplatebased MEMS resonators based MEMS resonators. *Mechanical Systems and Signal Processing, 109*, 220-234. doi:https://doi.org/10.1016/j.ymssp.2017.11.043

Hsiao, K. M. and Hou, F. Y. (1987). Nonlinear finite element analysis of elastic frames. *Computers & structures*, 693-701.

Mohammadi, H. and Mahzoon, M. (2013). Thermal effects on postbuckling of nonlinear microbeams based on the modified strain gradient theory. *Composite Structures, 106*, 764-776.

Nguyen, D. K. and Bui, V. T. (2017). Dynamic Analysis of Functionally Graded Timoshenko Beams in Thermal Environment Using a Higher-Order Hierarchical Beam Element. *Mathematical Problems in Engineering*, 1-12.

Tessler, A. and Dong, S. B. (1981). On a hierarchy of conforming Timoshenko beam elements. *Computers and Structures*, 335–344.

Wang, Y.-G., Lin, W.-H. and Liu, N. (2015). Nonlinear bending and post-buckling of extensible microscale beams based on modified couple stress theory. *Applied Mathematical Modelling, 39*(1), 117-127.

Xia, W., Wang, L. and Yin, L. (2010). Nonlinear non-classical microscale beams: static bending, postbuckling and free vibration. *International Journal of Engineering Science, 48*(12), 2044-2053.

Yang, F. A. C. M., Chong, A. C. M., Lam, D. C. C. and Tong, P. (2002). Couple stress based strain gradient theory. *International journal of solids and structures*, 2731-2743.

Younis, M. I. (2011). *MEMS linear and nonlinear statics and dynamics* (Vol. 20). Binghamton, New York: Springer Science & Business Media.